micromod Partikeltechnologie GmbH

modular designed particles

Publications and Reviews

Technological Applications

Implementation in Life Sciences

sicastar®

silica based nano and micro particles

www.micromod.de

Product overview

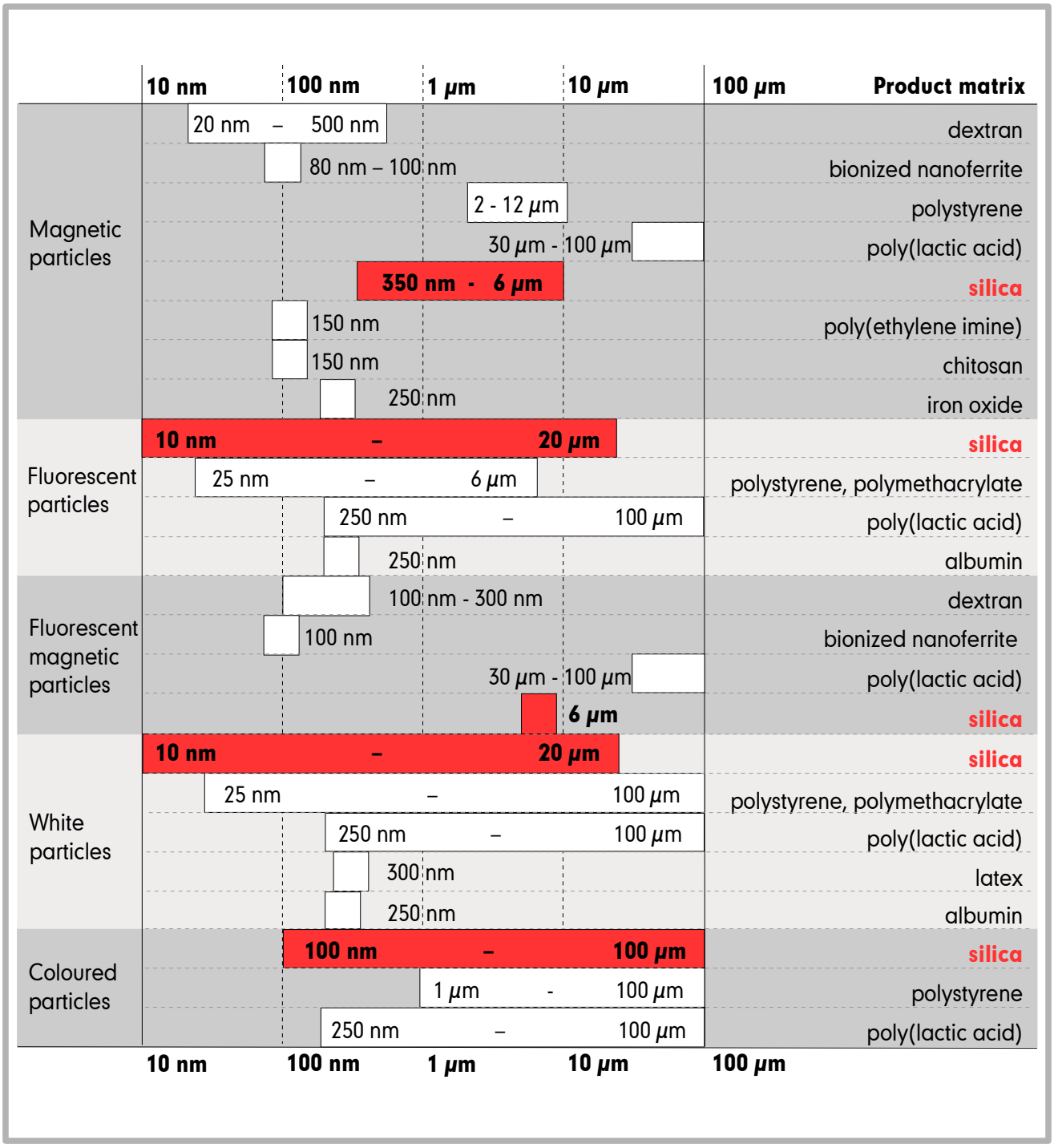

micromod Partikeltechnologie GmbH
Friedrich-Barnewitz-Straße 4, D-18119 Rostock
Tel.:+49 381/54 34 56 10, Fax: +49 381/54 34 56 20
Technical Support Tel.: +49 381/54 34 56 14
E-mail: info@micromod.de, Internet: www.micromod.de

page

Contents

1 Introduction

In June 1994, the chemist Dr. Joachim Teller and the physicist Fritz Westphal founded micro caps Entwicklungs- und Vertriebs GmbH located in Rostock, since 1999 being well-known as micromod Partikeltechnologie GmbH. The micromod Partikeltechnologie GmbH is a technology-oriented company with focus on the development and production of monodisperse micro- and nanoparticles. These particles are made from different materials, in different sizes and with a large variety of physical and chemical modifications.
This booklet sets the focus on the multifaceted studies, that our customers have performed with sicastar®- micromod's silica particles.

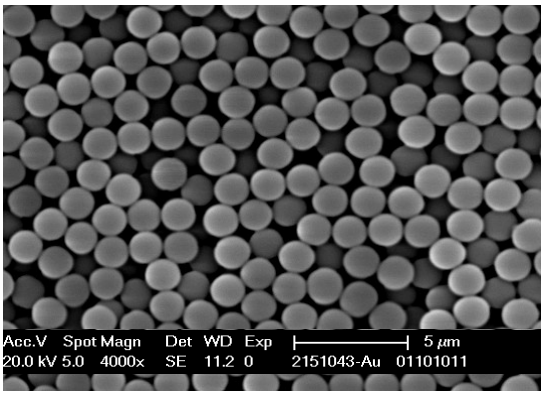

Figure 1: Transmission electron microscopy image of 1.5 µm sicastar® particles

Our sicastar® products are available as amorphous silica particles in the size range of 10 nm to 1.5 µm with a density of 2.0 g/cm³. These particles are prepared according to a modified Stoeber process [1] by hydrolysis of orthosilicates and related compounds as monodisperse and nonporous particles. They have a hydrophilic surface with terminal Si-OH-bonds.

Micron-sized porous sicastar® particles are provided with adjusted diameters between 3 and 20 microns and a density of 1.8 g/cm³. These larger particles have broader size distributions.
All sicastar® products are extremely stable in organic solvents and in aqueous buffers. The silica particles with diameters larger than 200 nm can easily be separated by simple sedimentation or centrifugation; particles with diameters smaller than 200 nm can be separated by ultracentrifugation or washed by size exclusion chromatography (e.g. desalting columns) or ultrafiltration/dialysis.

The sicastar® particles are designed with the surface functionalities OH (plain), NH_2, COOH, CHO, SO_3H, SH, N-hydroxysuccinimide (NHS) or epoxy for the covalent binding of proteins, antibodies or other molecules. They are also available with covalently bound proteins on the surface (e.g. avidin, streptavidin, protein A, albumin) or can be provided with customer-specific covalently bound antibodies, peptides or other molecules on request. sicastar® particles are offered with the nickel(II) chelator nitrilotriacetic acid (NTA) or ready-to-use with the corresponding nickel complex (Ni-NTA) for the binding of histidine labeled proteins. Furthermore they are suitable for the complexation of other metal ions after introduction of special chelators on the particle surface (e.g. EDTA or DTPA). sicastar® particles are provided with gold labeling in our standard assortment or with other metal labelings (e.g. Pt, Pd, Ag) on request.

For special applications sicastar® particles can be modified with other inorganic structures (co-titania or co-alumina) or with various hydrophobic/ organic surfaces (acrylate, trimethylsilyl (TMS) or octadecyl (C18)).
sicastar® particles are also available with fluorescence properties for special detection purposes, e.g. in flow cytometry, membrane checks or flow investigations. The fluorescent sicastar® particles contain a high amount of covalently bound fluorescence dye in the silica matrix and are extremely stable in organic solvents and buffers.

No toxic effects come from the covalently bound fluorescence dyes [2]. The particles have a hydrophilic surface with terminal Si-OH-bonds and are available with the surface functionalities NH_2 and COOH for the covalent binding of proteins, antibodies, oligonucleotides, enzymes or other molecules.
sicastar® particles are available with red fluorescence (sicastar®-redF, excitation: 569 nm, emission: 585 nm), green fluorescence (sicastar®-greenF, excitation: 485 nm, emission: 510 nm) and blue fluorescence (sicastar®-blueF, excitation: 354 nm, emission: 450 nm). sicastar® particles with special fluorescence dyes can be made on customer's request.

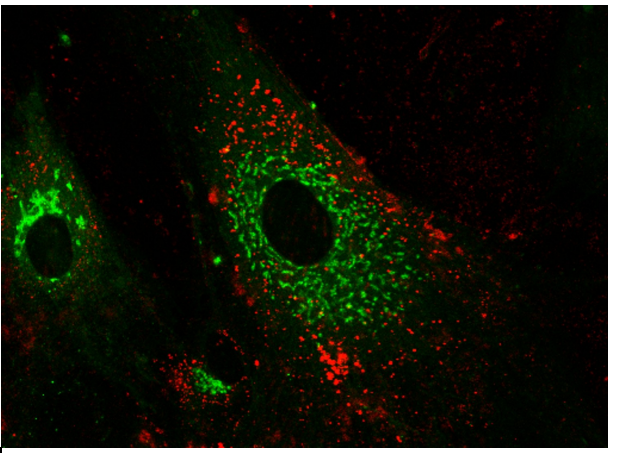

Figure 2: Uptake of 100 nm plain sicastar®-redF, particles in human mesenchymal stem cells (Golgi apparatus green coloured)

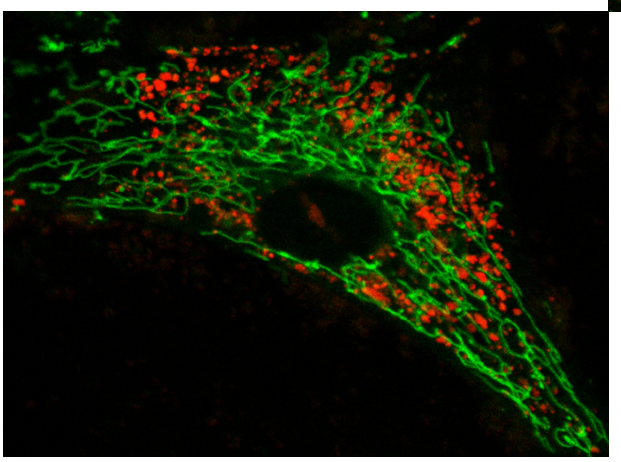

Figure 3: Uptake of 50 nm carboxylated sicastar®-redF particles in human mesenchymal stem cells (Mitochondria green coloured)

Magnetic silica particles are divided into sicastar®-M particles with mean diameters of 350 nm or 1.5 µm and cluster-typed magnetic silica particles (sicastar®-M-CT), that consist of aggregates in the size range of 3 - 10 µm with a mean diameter of 6 microns .

The magnetic silica particles are produced by hydrolysis of orthosilicates in the presence of magnetite. sicastar®-M particles have monomodal size distributions, while the cluster-typed sicastar®-M-CT particles have a broader size distribution. Both types of magnetic silica particles have a hydrophilic surface with terminal Si-OH-bonds and can easily be separated with conventional permanent magnets. They are extremely stable in organic solvents and at high temperatures. The magnetic silica particles are designed with the surface functionalities OH (plain), NH_2, COOH, SH, N-hydroxysuccinimide (NHS) and epoxy for the covalent binding of proteins, antibodies or other molecules, and are available with covalently bound proteins (avidin, streptavidin, protein A, albumin) or biotin. They can be offered with the nickel(II) chelator nitrilotriacetic acid (NTA) or ready to use with the corresponding nickel complex (Ni-NTA) for the binding of histidine labeled proteins. The magnetic silica particles are available with a hydrophobic octadecyl (C18) surface, and can be delivered with an organic polymer shell (core-shell method) on request.

sicastar® particles have a large variety of applications especially in the field of life sciences, device developments and quality control, as analytical tools and defined model particles for different processes. The following sections provide a review of third party papers on applications of sicastar® particles

- in toxicity studies of nanoparticles
- as analytical tools
- as model particles in geo- and astrophysics
- for the formation of colloidal crystals
- as model particles in optics
- for magnetic separation of radionuclides or other metal ions.

References

[1] Stöber W, Fink A, Bohn E. Controlled Growth of Monodisperse Silica Spheres in the Micron Size Range. J Colloid Interface Sci 1968;26:62-69.

[2] Teller J, Grüttner C, Rudershausen S, Westphal F, Verfahren zur Herstellung gefärbter und fluoreszenter Polykieselsäure-Partikel. 2000. EP 1036763

2 Toxicity studies with amorphous sicastar® particles

Prof. Dr. Joachim Rychly (University of Rostock, Department of Cell Biology),

Dr. Cordula Grüttner (micromod Partikeltechnologie GmbH)

Amorphous silica nanoparticles gain increasing popularity for industrial and therapeutic applications. They are widely used in many consumer products such as cosmetics, food, and medicine because of their useful properties, including straightforward synthesis, relatively low cost, easy separation and easy surface modification. In comparison to conventional materials with submicron size, nanoparticles show unique properties such as high levels of electrical conductivity, tensile strength and chemical reactivity. However, recent studies have found that silica nanoparticles induce various toxic effects [1]. Some years ago several international research programs initiated a systematic study of the toxicity issues of nanoparticles. A comprehensive Japanese toxicity study with amorphous silica nanoparticles started in 2008 and was supported by the Ministry of Health, Labour, and Welfare of Japan. For this ongoing study micromod's amorphous sicastar® particles in the size range of 30 nm to 1 µm were chosen as model particles with high demands on reproducibility in size distribution, surface charge and fluorescence properties.

Here we will discuss recent data concerning toxicity studies *in vitro* and *in vivo* and ask whether toxic effects depend on size or chemical surface modifications.

2.1 *In vitro* and *in vivo* cytotoxicity studies

A dose and time dependent cytotoxicity of 15 nm and 48 nm SiO_2 nanoparticles was found in a human bronchoalveolar carcinoma cell line [2]. In a human keratinocyte cell line (HaCaT**),** a size dependent effect of silica particles on the level of reactive oxygen species (ROS), leading to DNA damage was observed [3]. The exposure of these cells to 70 nm silica particles induced an elevated level of ROS, whereas bigger particles with sizes of 300 nm and 1 µm had no effect. Because only 70 nm particles entered the cell nucleus, nuclear localization appears to be important for a cytotoxic effect [4]. This is supported by another study in the murine macrophage cell line RAW264.7 [5]. Particles with amine or carboxyl groups on the surface did not enter the nucleus and had a low toxic effect, whereas plain particles were found in the nucleus and induced a toxic effect. Silica particles had also cytotoxic effects in various other types of cells.

In an endothelial cell line (EAHY926) a similar size dependent toxic effect was observed with higher effects of smaller particles compared with particles sized 100 or 300 nm [6]. Similarly, in murine epidermal Langerhans cells, cellular uptake and cytotoxicity increased with reduction in particle size [7]. However, whether a defined size of nanoparticle induces cytotoxicity depends on the cell type. In contrast to the cells mentioned above, sicastar® particles with sizes between

30 and 70 nm did not induce cytotoxicity in a THP-1 human macrophage cell line, whereas larger particles of 300 nm and 1 µm induced toxic effects in these cells [6]. The surface functionalization of the 1 µm particles with NH_2, SO_3H or aldehyde groups significantly suppressed the cytotoxicity in comparison to the non-functionalized (plain) or carboxylated particles [8].

The sensitivity of a cell type to nanoparticles also depends on the interaction with other cells. Cells in a co-culture of an epithelial cell line with an endothelial cell line were less sensitive to toxic effects of differently sized nanoparticles (30, 70, 300 nm) compared with the effects in separated monocultures of both cell types [9].

There are a number of studies that examined the cytotoxicity of sicastar® particles *in vivo*. Nabeshi et al. analyzed biodistribution and biological effects in systemic level using 70 nm, 300 nm and 1 µm fluorescent sicastar® particles by optical imaging analysis. Intense fluorescence was observed near the liver in all silica-particle treated mice. This signal migrated to near the intestinal tract with time. Imaging of dissected liver from 300 nm and 1 µm sicastar® treated mice revealed that intense fluorescence was observed around the gall bladder. In contrast 70 nm sicastar® derived fluorescence was observed throughout dissected liver [4] (Figure 1).

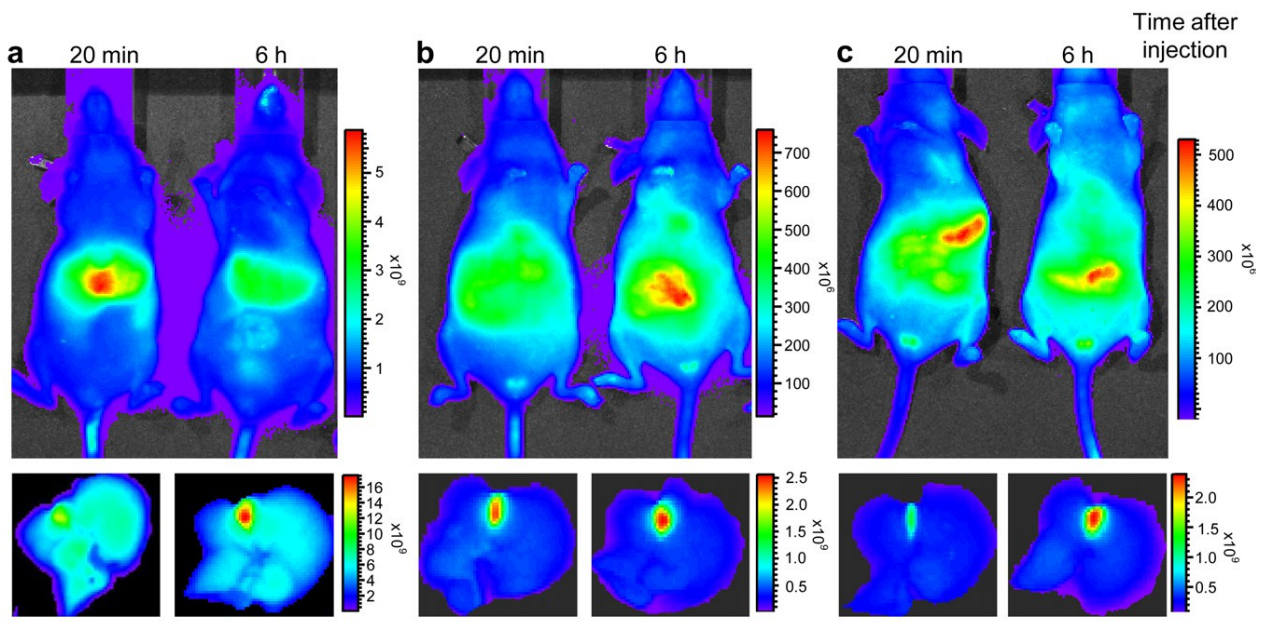

Figure 1: Biodistribution analysis of fluorescent sicastar® particles of different diameters (a) 70 nm, b) 300 nm and c) 1 µm) by optical imaging in live mice and excised liver. DY676-labeled sicastar® particles (100 mg/kg) were intravenously injected into female hairless mice. Twenty min and 6 h after injection, optical images were acquired using a Xenogen IVIS 200 imaging system [4].

In mice, 70 nm particles were chronically injected into several organs for 4 weeks. Histological analyses revealed toxic effects in liver and spleen, whereas kidney, lung, brain, and heart remained unaffected [10]. Larger particles with sizes of 300 nm or 1 µm were less harmful [11]. Examination of liver toxicity using surface modified particles correlated with the findings *in vitro*.

Surface modification with amino groups and carboxyl groups had a much weaker cytotoxic effect in the mouse liver compared with unmodified particles when intravenously injected [12]. Liver injury induced by nanoparticles involves hepatocytic necrosis, increased serum transaminases, and inflammatory cytokines [13]. The same dependency of toxicity on particle size and chemical surface modifications were found, when nanoparticles were intravenously injected in pregnant mice. The nanoparticles crossed the placenta barrier and induced neurotoxicity and other pregnancy complications. However, these complications were not found when larger particles with a size of 300 nm or 1 µm were used and after modification of the surface with amino- and carboxyl groups [14]. The toxic effects of 70 nm nanoparticles in mice may be caused by severe disturbances of the blood clotting system. A consumptive coagulopathy was observed which was dependent on the interaction of the nanoparticles with the intrinsic coagulation factor XII [15]

Some studies examined toxic effects of nanoparticles when administered together with drugs. In a mouse model the synergistic effects of nanoparticles with the anti-tumor agent cisplatin and the herbicide paraquat were studied [11]. While the drugs and particles alone were nontoxic, the combined administration of cisplatin or paraquat with particles induced toxicity. Again, the effect was size dependent, because particles with a size of 300 nm or 1 µm had no toxic effect.

2.2 Physiological and pathophysiological effects of sicastar® particles

Beside toxic effects of nanoparticles to cells *in vitro* or harmful effects *in vivo* that might lead to organ failure, attention has been drawn to the control of physiological process in the organism by administered nanoparticles. Obviously, distinct effects of nanoparticles have been observed in the immune system. In context with the induction of an inflammation, IL-1β secretion in human macrophages was studied after incubation with silica nanoparticles [16]. Larger particles (1 µm) induced higher levels of IL-1β secretion than smaller ones. Also the surface characteristics of the particles influenced the cellular response. Although unmodified particles and particles modified with amino- or carboxyl groups entered the macrophages to the same extent, surface modified particles dramatically suppressed the release of IL-1β. In lung epithelial cells and endothelial cells, nanoparticles induced an increased secretion of IL-8, which indicates an inflammatory response [17], [18]. In a mouse model for atopic dermatitis, simultaneous administration of the antigen together with nanoparticles enhanced the immunological response, which indicates an adjuvant activity of the particles [19]. The authors observed an excessive systemic IL-18 production and Th2 cell response. In addition, locally in the skin lesion, IL-18 and thymic stromal lymphopoeitin secretion increased. These effects were size dependent and increased with decreasing particle size. A mouse model was used to examine the role of nanoparticles in allergic responses [20]. Mice were intranasally exposed to nanosilica particles plus ovalbumin and the levels of anti-ovalbumin antibodies were analysed. Smaller nanoparticles (70 nm, 30 nm) induced higher levels of specific antibodies in blood plasma than did larger particles (300 nm, 1 µm). In addition, *in vitro* particles together with ovalbumin induced higher Th2-type cytokines in

mouse splenocytes than ovalbumin alone. These results indicate that silica particles can induce Th2-type allergic responses. Because macrophages appeared sensitive to nanoparticles, the effect of silica particles on the development of the bone resorbing osteoclasts was studied [21]. However, at sub-toxic doses, no changes in differentiation and number of cells were observed.

2.3 Biomarkers to analyse biological responses after exposure to silica nanoparticles

To develop a risk assessment system for the application of nanoparticles, a study using a proteomics based approach analysed the plasma proteins after administration of nanoparticles [22]. The authors identified haptoglobin, one of the acute phase proteins, as suitable candidate for a biomarker. Haptoglobin was significantly elevated in plasma of mice exposed to silica nanoparticles with a diameter of 70 nm compared to normal mice and those exposed to silica particles with a diameter of 1 µm. in addition, other acute phase proteins, like C-reactive protein (CRP) and serum amyloid A (SAA) were also elevated in plasma of particle treated mice, which all might be useful parameters for assessing the risk of exposure to silica nanoparticles. In a similar approach, the authors identified hemopexin as a potential biomarker [23]. The levels of hemopexin in the plasma of mice increased as the silica particle size decreased and were dependent on the surface characteristics of the particles.

All these studies demonstrate the significant influence of particle size and surface modification on the toxicity of silica nanoparticles. These aspects have to be considered carefully at the application of nanoparticles in products, that interact with living organisms and especially with the human body.

References

[1] Napierska D, Thomassen LC, Lison D, Martens JA, Hoet PH. The Nanosilica hazard: another variable entity. Part Fibre Toxicol. 2010;7:39(32 pp).

[2] Lin W, Huang YW, Zhou XD, Ma Y. In vitro toxicity of silica nanoparticles in human lung cancer cells. Toxicol. Appl. Pharmacol. 2006;217:252-259.

[3] Nabeshi H, Yoshikawa T, Matsuyama K, Nakazato Y, Tochigi S. Amorphous nanosilica induce endocytosis-dependent ROS generation and DNA damage in human keratinocytes. Particle and Fibre Toxicology 2011;8(1):1-10.

[4] Nabeshi H, Yoshikawa T, Matsuyama K, Nakazato Y, Matsuo K, Arimori A et al. Systemic distribution, nuclear entry and cytotoxicity of amorphous nanosilica following topical application. Biomaterials 2011;32:2713-2724.

[5] Nabeshi H, Yoshikawa T, Arimori A, Yoshida T, Tochigi S, Hirai T et al. Effect of surface properties of silica nanoparticles on their cytotoxicity and cellular distribution in murine macrophages. Nanoscale Res Lett 2011;6:93(6 pp).

[6] Napierska D, Thomassen LC, Rabolli V, Lison D, Gonzalez L, Kirsch-Volders M et al. Size-dependent cytotoxicity of monodisperse silica nanoparticles in human endothelial cells. Small 2009;5(7):846-853.

[7] Nabeshi H, Yoshikawa T, Matsuyama K, Nakazato Y, Arimori A, Isobe K et al. Size-dependent cytotoxic effects of amorphous silica nanoparticles on Langerhans cells.

Pharmazie 2010;65:199-201.

[8] Morishige T, Yoshioka Y, Inakura H, Tanabe A, Yao X, Tsunoda S-i et al. Cytotoxicity of amorphous silica particles against macrophage-like THP-1 cells depends on particle-size and surface properties. Pharmazie 2010;65:596-599.

[9] Kasper J, Hermanns MI, Bantz C, Maskos M, Stauber R, Pohl C et al. Inflammatory and cytotoxic responses of an alveolar-capillary coculture model to silica nanoparticles: comparison with conventional monocultures. Part Fibre Toxicol. 2011;8:6(16 pp).

[10] Nishimori H, Kondoh M, Isoda K, Tsunoda S-i, Tsutsumi Y, Yagi K. Histological analysis of 70-nm silica particles-induced chronic toxicity in mice. Eur. J. Pharm. Biopharm. 2009:626-629.

[11] Nishimori H, Kondoh M, Isoda K, Tsunoda S-i, Tsutsumi Y, Yagi K. Influence of 70 nm silica particles in mice with cisplatin or paraquat-induced toxicity. Pharmazie 2009;64:395-397.

[12] Isoda K, Hasezaki T, Kondoh M, Tsutsumi Y, Yagi K. Effect of surface charge on nano-sized silica particles-induced liver injury. Pharmazie 2011;66(4):278-281.

[13] Lu X, Tian Y, Zhao T, Xiao S, Fan X. Integrated metabonomics analysis of the size-response relationship of silica nanoparticles-induced toxicity in mice. Nanotechnology 2011;22(5):055101.

[14] Yamashita K, Yoshioka Y, Higashisaka K, Mimura K, Morishita Y, Nozaki M et al. Silica and titanium dioxide nanoparticles cause pregnancy complications in mice. Nature Nanotechnol. 2011;6(5)321-328.

[15] Nabeshi H, Yoshikawa T, Matsuyama K, Nakazato Y, Arimori A, Isobe M et al. Amorphous nanosilicas induce consumptive coagulopathy after systemic exposure. Nanotechnology 2012;23:045101 (8pp).

[16] Morishige T, Yoshioka Y, Inakura H, Tanabe A, Yao X, Narimatsu S et al. The effect of surface modification of amorphous silica particles on NLRP3 inflammasome mediated IL-1ß production, ROS production and endosomal rupture. Biomaterials 2010:6833-6842.

[17] Kasper J, Hermanns MI, Bantz C, Koshkina O, Lang T, Maskos M et al. Interactions of silica nanoparticles with lung epithelial cells and the association to flotillins. Arch Toxicol. 2013;87(6):1053-1065

[18] Kasper J, Hermanns MI, Bantz C, Utech S, Koshkina O, Maskos M et al. Flotillin-involved uptake of silica nanoparticles and responses of an alveolar-capillary barrier in vitro. Eur. J. Pharm. Biopharm. 2013;84:275-287.

[19] Hirai T, Yoshikawa T, Nabeshi H, Yoshida T, Tochigi S, Ichihashi K-i et al. Amorphous silica nanoparticles size-dependently aggravate atopic dermatitis-like skin lesions following an intradermal injection. Part Fibre Toxicol. 2012;9:3(11 pp).

[20] Yoshida T, Yoshioka Y, Fujimura M, Yamashita K, Higashisaka K, Morishita Y et al. Promotion of allergic immune responses by intranasally-administrated nanosilica particles in mice. Nanoletters 2011;6:195(6 pp).

[21] Nabeshi H, Yoshikawa T, Akase T, Yoshida T, Tochigi S, Hirai T et al. Effect of amorphous silica nanoparticles on in vitro RANKL-inducend osteoclast differentiation in murine macrophages. Nanoscale Res. Lett. 2011;6:464(5 pp).

[22] Higashisaka K, Yoshioka Y, Yamashita K, Morishita Y, Fujimura M, Nabeshi H et al. Acute phase proteins as biomarkers for predicting the exposure and toxicity of nanomaterials. Biomaterials 2011;32:3-9.

[23] Higashisaka K, Yoshioka Y, Yamashita K, Morishita Y, Pan H, Ogura T et al. Hemopexin as biomarkers for analyzing the biological responses associated with exposure to silica nanoparticles. Nanoscale Res. Lett. 2012;7:555(9 pp).

3 Sicastar® particles as analytical tools

Dr. Cordula Grüttner (micromod Partikeltechnologie GmbH)

Functionalized silica particles are a versatile platform for the binding of target molecules for innovative analytical applications in the medical, chemical, biochemical, ecological and electronic industries. The following sections describe a selection of highly specialized analytical applications of silica particles in these diverse fields.

3.1 Screening of potential cancer therapeutics

There is a strong experimental and clinical evidence, that the plasminogen activator system encompassing the serine protease uPA and its cell surface receptor uPAR (CD87) is associated with tumor cell invasion and metastasis. Increased levels of uPA and uPAR have been found in primary tumor tissues of patients afflicted with solid tumors [1]. Guthaus et al. designed an efficient analytical system with 10 μm sicastar® particles to investigate the interaction between the urokinase-type plasminogen activator (uPA) and the uPA receptor (uPAR) by flow cytofluorometry. Therefore the carboxylated particles were conjugated with the serine protease uPA employing the carbodiimide/ N-hydroxysuccinimide chemistry. This system was also used to test synthetic uPAR antagonists as potential cancer therapeutics [1-2]. Independent of its proteolytic activity the uPA protein content in tumor tissue is of even higher prognostic relevance indicating a prominent role of both the proteolytic action of uPA and the uPA/uPAR interaction in tumor invasion.

3.2 Analysis of gene regulation functions

The genomic DNA of all eukaryotes is packed in the cell nucleus in the form of chromatin. It has been well established that beside compaction of the important amount of genomic DNA in the restricted nuclear volume, the chromatin organization is the key element in the control of gene expression. Its most abundant part is represented by association of the DNA with a specific class of proteins - the histones, forming a basic repetitive unit of the chromatin – the nucleosome. Carboxylated sicastar® particles with a diameter of 1.5 μm were conjugated with digoxigenin to study the concentration dependent and external stress dependent histone octamer stability in native and reconstituted nucleosomal arrays to get information on the gene regulation function of the chromatin [3].

3.3 Nucleic acid analysis

DNA functionalized nanoparticles have been recognized as attractive nanotools in medical and food biomolecular diagnostics because of their inherent specific properties including DNA detection through hybridization, aptamer based ligand detection, and DNA mediated nanoparticle aggregation and disaggregation. These analytical applications require an accurate quantification of low numbers of anchored DNA biomolecules on individual nanoparticles. In

order to accurately determine such low numbers of immobilized single stranded DNA (ssDNA) molecules at a single nanoparticle surface Delport et al. proposed an integrated approach combining classic single molecule confocal microscopy with a modified total internal reflection fluorescence microscopy [4]. Therefore silica nanoparticles with a diameter of 250 nm and COOH groups on the surface were covalently linked with various amounts of fluorescence-labelled ssDNA and used as model particles for the development of the methodology [4].

In recent years, DNA chip-based assays have become a familiar approach suitable for a broad range of applications such as expression analysis and genotyping. The expansion of DNA chip technology has encouraged the rapid development of optimal oligonucleotide immobilization methods to prevent errors in the directed covalent DNA attachment. Thus Penchovsky et al. have developed a new method of end-specific covalent photo-dependent immobilization of synthetic DNA to magnetic silica and polystyrene particles [5]. This photo-dependent DNA immobilization should allow the programmed immobilization of DNA to beads in micro-flow reactors [6]. Therefore magnetic silica particles (sicastar®-M) or magnetic polystyrene particles (micromer®-M) with amino groups on the surface were functionalized with the photo-reactive crosslinking agent 4-nitrophenyl 3-diazopyrovate for the binding of 3'- or 5'-end amino-modified ssDNA. This method should allow the selective addressing of beads placed in different positions in micro-flow reactors using a photo-lithographic mask and the individual and parallel analysis of the DNA-labelled beads [5].

3.4 Magnetic pre-concentration of heavy metal ions for quantitative analysis

Magnetic silica particles are also interesting tools for the pre-concentration of metal ions to achieve suitable concentrations for their quantitative analysis. Heavy metal ions are commonly found in raw or treated drinking water as it enters the distribution system. These metal ions may also appear in the consumer's tap water as a result of corrosion of pipes. Mandil et al. used thiolated magnetic silica particles (sicastar®-M) with a diameter of 1.5 µm for the pre-concentration of mercury(II) and lead(II) for the stripping voltammetric determination of these heavy metal ions. The heavy metal ions in the trap water sample bind to the surface of the thiolated sicastar®-M particles. After magnetic separation the particles were suspended in acidic media to release the metal ions for analysis [7].

3.5 Encoding with fluorescent silica particles in combinatorial chemistry

Chemical library technology plays a central role in research areas such as drug discovery and gene screening. The most powerful combinatorial library synthesis method is the "split and mix" synthesis on insoluble microscopic beads (solid support beads). Battersby et al. have used 1 µm sicastar® particles, that contain combinations of one to three fluorescent dyes, for the development of a colloidal barcoding technology. In a split and mix synthesis, a large number of solid support beads is partitioned into several vessels, a different monomer (e.g. nucleic acid, sugar or amino acid) is reacted with each portion, and then the beads are recombined to

complete the cycle. The split and mix process is repeated for a chosen number of cycles, resulting in a chemical library, ideally consisting of all monomer combinations. One type of fluorescent sicastar® particle was used as code for each different reaction and every solid support bead received multiple copies at each reaction. Each type of fluorescent silica particle is distinguished by its specific combination of fluorescent dyes. Thus the efficient use of relatively few dyes leads to an enormous amount of information, that can easily be recorded by standard fluorescence microscopy techniques [8] (Figure 1).
Another application of fluorescent sicastar® nanoparticles is the design of molecule arrays [9].

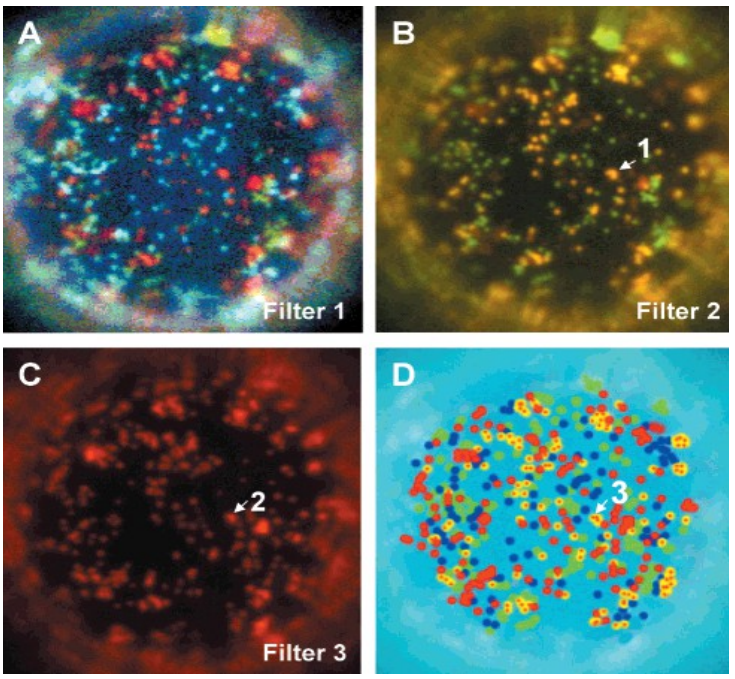

Figure 1: Fluorescence microscopy is used to read the colloidal barcode that identifies the chemical structure of the compound on a support bead in a library. (A-C) The bead is analyzed under three different filters and the individual dyes present within each reporter are identified. (D) A schematic representation showing the combinations of dyes present in each reporter [8].

3.6 Analysis of particle interactions with ecological systems

Artificial silica nanoparticles provide the advantage of adjustable physical properties such as diameter and surface charge. Therefore sicastar® particles served as model particles for studies of the interactions with ecological systems. Boenigk et al. investigated the influence of suspended particles with different diameters between 100 nm and 15 µm on the growth of a freshwater flagellate community as model microorganisms [10]. They found that the particle size of suspended sediments is an important parameter, influencing the clearance rates of the flagellates. While the clearance rates were only slightly affected by 3 µm sicastar® particles, smaller and larger particles led to a significant decrease of the clearance rates of the flagellates [10]. Sicastar® particles with a constant diameter of 800 nm and different zetapotentials served as artificial model particles to study the heavy metal toxicity and bioavailability of dissolved nutrients to a bacterivorous flagellate. The toxicity of cadmium(II) and mercury(II) was found to decrease in the presence of suspended particles. An increasing negative surface charge of the particles resulted in an increase of the cadmium(II) toxicity, but had no significant effect on the mercury(II) toxicity [11].

3.7 Analysis of colloidal dispersions

Another application of silica nanoparticles is the analysis of colloidal dispersions by determination of blockade rates of tunable nanopores (TN) in elastic membranes. Willmott et al. studied the blockade rates for carboxylated or aminated 200 nm and 500 nm silica particles and found that the changes in particle mobility correlate with changes of the solution pH [12]. The TN technology was shown to be a timely and efficient method for the analysis of the concentration of an unknown specimen, once a calibration using a particle set of known concentration had been performed. Furthermore the particle electrophoretic mobility can be studied at the level of individual particles [12].

References

[1] Guthaus E, Bürgle M, Schmiedeberg N, Hocke S, Eickler A, Kramer MD et al. uPA-Silica-Particles (SP-uPA): A novel analytical system to investigate uPA-uPAR-interaction and to test synthetic uPAR-antagonists as potential cancer therapeutics. Biolog. Chem. 2002;383(1):207-216.

[2] Guthaus E, Schmiedeberg N, Bürgle M, Magdolen V, Kessler H, Schmitt M. The urokinase receptor (uPAR, CD87) as a target for tumor therapy: uPA-Silica-Particles (SP-uPA) as a new tool to assess synthetic peptides to interfere with uPA/uPA-receptor interaction (Review). Recent Results Cancer Res. 2003;162:3-14.

[3] Claudet C, Angelov D, Bouvet P, Dimitrov S, Bednar J. Histone octamer instability under single molecule experiment conditions. J. Biol. Chem. 2005;280(20):19958-19965.

[4] Delport F, Deres A, Hotta J-i, Pollet J, al. e. Improved methods for counting DNA molecules on biofunctionalized nanoparticles. Langmuir 2010;26(3):1594-1597.

[5] Penchovsky R, Birch-Hirschfeld E, McCaskill JS. End-specific covalent photo-dependent immobolisation of synthetic DNA to paramagnetic beads. Nucleic Acids Research 2000;28(22):98.

[6] Penchovsky R, McCaskill JS. Cascadable hybridisation transfer of specific DNA between microreactor selection modules. DNA 7, LNCS 2340; N. Jonoska and N.C. Seeman (Eds.) Springer Verlag Heidelberg 2002:46-56.

[7] Mandil A, Idrissi L, Amine A. Stripping voltammetric determination of mercury(II) and lead(II) using screen-printed electrodes modified with gold films, and metal ion preconcentration with thiol-modified magnetic particles. Microchim Acta 2010;170:299-305.

[8] Battersby BJ, Bryant D, Meutermans W, Matthews D, Smythe ML, Trau M. Toward Larger Chemical Libraries: Encoding with Fluorescent Colloids in Combinatorial Chemistry. J Am Chem Soc 2000;122(9):2138-2139.

[9] Howorka S, Pammer P. Molecule arrays and method for producing the same. WO/2005/025737 2005.

[10] Pfandl K, Boenigk J. Stuck in the mud: suspended sediments as a key issue for survival of chrysomonad flagellates. Aquat. Microb. Ecol. 2006;45:89-99.

[11] Boenigk J, Wiedlroither A, Pfandl K. Heavy metal toxicity and bioavailability of dissolved nutrients to a bacterivorous flagellate are linked to suspended particle physical properties. Aquat. Toxicol. 2005;71:249-259.

[12] Willmott GR, Vogel R, Yu SSC, Groenewegen LG, Roberts GS, Kozak D et al. Use of tunable blockade rates to investigate colloidal dispersions. J Phys Condens Matter 2010;22:454116.

4 sicastar® particles in geo- and astrophysics

Dr. Rainer Schräpler (Technical University Braunschweig, Institute for Geophysics and Extraterrestrial Physics),

Dr. Cordula Grüttner (micromod Partikeltechnologie GmbH)

Long-duration experiments with clouds of microparticles are interesting research objects ranging from the simulation of aerosol behavior in Earth's atmosphere to the formation of planets in the early solar system. It is, however, even under microgravity conditions, impossible to sustain a cloud of free-floating, microscopic particles for an extended period of time, due to thermal diffusion and due to unavoidable external accelerations. As a part of the ICAPS (Interactions in Cosmic and Atmospheric Particle Systems) project for the International Space Station (ISS) a three-dimensional trap for clouds of microparticles should be developed. This trap for dust clouds is required to prevent the particle drift caused by thermophoresis and thermal creep. Because this drift terminates experiments by driving the particles to the chambers walls.

Thermal diffusion provides a source of relative velocities between the dust grains and drives the particle coagulation. Steinbach et al. used 1 μm plain sicastar® particles as model particles for dust, and developed a particle trap by using the photophoretic effect [1].

Highly porous materials made of micron-sized particles have attracted significant attention. One reason is that these materials allow the relation of microscopic properties such as adhesion and friction forces between individual particles to macroscopic quantities such as compressibility. One example for the interest in both, individual particle contact as well as properties of agglomerates consisting of these particles, is the formation of planetesimals. Furthermore the behavior of particle agglomerates is crucial in particle filtration, because the performance of fibrous and membrane filters is often limited by the formation of dust cakes. Blum and Schräpler used plain 1.5 μm sicastar® particles for the development of macroscopic agglomerates formed by ballistic hit-and-stick deposition [2]. The agglomerates, produced with this experimental method, have a volume filling factor of ϕ=0.15, matching very closely the theoretical value for random ballistic deposition. They are mechanically stable against unidirectional compression of up to 500 Pa. For pressures above that value, the volume filling factor increases to a maximum of ϕ=0.33 for pressures above 10^5 Pa. The tensile strength of slightly compressed samples (ϕ=0.2) is 1000 Pa. Blum et al. found that the maximum compression, equivalent to the highest protoplanetary impact velocities of ~50 ms^{-1}, increases the packing density to 0.20–0.33. Tensile strength measurements with the laboratory samples yielded values in the range of 200–1100 Pa for slightly compressed samples. The review of packing densities and tensile strengths found for primitive solar system bodies, e.g., for comets, primitive meteorites, and meteoroids showed a consistency between packing densities and tensile strengths of the laboratory samples with those from cometary origin [3].

Langkowski et al. varied the porosity of the dust aggregates to study the collision effects for aggregates with a smooth surface (porosities between 85% and 93%) in comparison to aggregates with a molded surface and a decreased porosity of 80%-85%. The molding of the aggregates was performed such that the radii of the local surface curvatures corresponded to the projectile radii. The experiments showed that impacts into the highest porosity targets almost always led to sticking, whereas for the less porous dust aggregates, consisting of monodisperse 1.5 μm sicastar® particles, the collisions with intermediate velocities and high impact angles resulted in the bouncing of the projectile with a mass transfer from the target to the projectile aggregate. For the impacts into smooth aggregates of sicastar® particles the depth of intrusion and the crater volume were measured. From these results some interesting dynamical properties could be derived, which can help to develop a collision model for protoplanetesimal dust aggregates [4].

In further experiments the collisional behavior of the dust aggregates of the 1.5 μm sicastar® particles was studied at velocities below and around the fragmentation treshold. Therefore two experimental setups with the same goal were developed: to study the effects of bouncing, fragmentation, and mass transfer in free particle-particle collisions. The first setup was an evacuated drop tower with a free-fall height of 1.5 m. The second setup was designed to study the effect of partial fragmentation (when only one of the two aggregates was destroyed) (Fig.1).

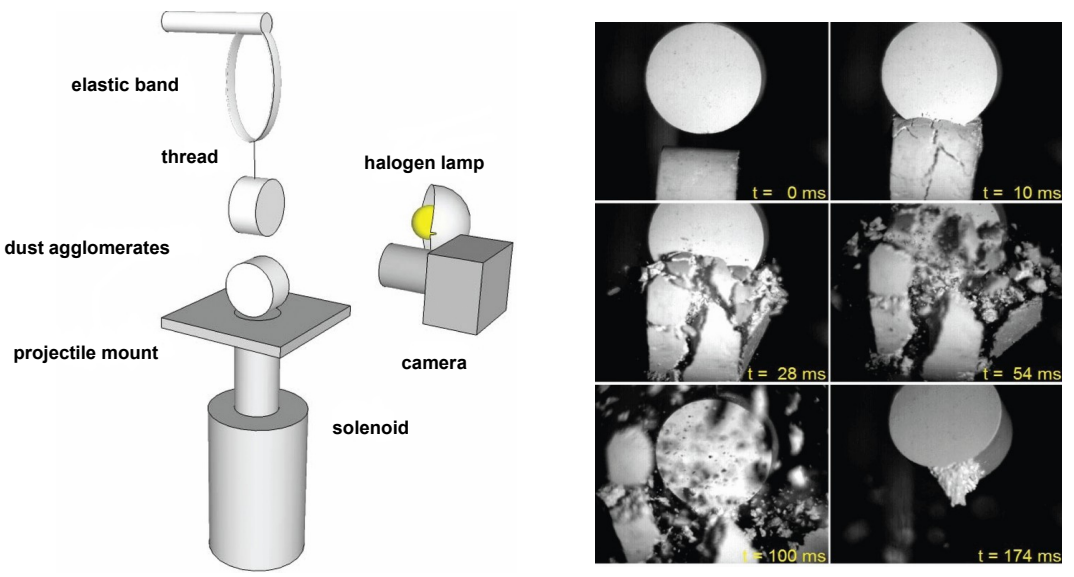

Figure 1. Experimental setup for collisions of the dust cylinders. The solenoid accelerates the lower aggregate, which collides with the upper aggregate (left). Image sequence, that illustrates the collision between the cylindrical samples with a collision velocity of 1 m/s (right) [5].

The measured critical energy for disruptive collisions was found to be at least two orders of magnitude lower than given in the literature. The accretion efficiency on the order of a few percentage points of the particle mass depends on the impact velocity and the sample porosity. These findings will have consequences for dust evolution models in protoplanetary disks as well as for the strength of large, porous planetesimal bodies [5].
Heim et al. used the highly porous agglomerates of 1.5 μm sicastar® particles, formed by random ballistic deposition, to analyze their compaction. The porous agglomerates were deformed inside

a scanning electron microscope (SEM) using the cantilever of an atomic force microscope (AFM). The applied force and structural deformations with single particle resolution could be obtained simultaneously. It was found that whole blocks of many particles move collectively upon compression. Within these blocks the relative positions of the particles remained fixed. This results in a discontinuous force-compression curve [6]. The analysis technique was further improved by implementation of a piezoelectric controlled nanomanipulator with increments of 5 nm in the rotational and 0.5 nm in the translational direction. This tool allows the precise positioning and movement of an AFM cantilever under SEM observation. The higher sensitivity of the method allows the study of different aspects of the deformation of dust-aggregate structure, e.g. the behaviour of single particle chains. These findings allow a deeper insight into mechanical properties of granular matter – the second most handled material by men [7].

The fluence of dust particles < 10 μm in diameter was recorded by impacts on aluminium foil of the NASA Stardust spacecraft during a close fly-by of comet 81P/Wild 2 in 2004. Initial interpretation of craters for impactor particle dimensions and mass was based upon laboratory experimental simulations using >10 µm diameter projectiles and the resulting linear relationship of projectile to crater diameter was extrapolated to smaller sizes. For the experimental proof of this extrapolation Price et al. [8] developed a new experimental calibration programme firing very small monodisperse silica projectiles (470 nm to 10 µm) at ~ 6 km s-1. Projectile materials were plain 10 μm sicastar® particles and smaller commercially available silica particles. The results show an unexpected departure from linear relationship between 1 and 10 µm. Using the new calibration, Price et al. could recalculate the size of the particle responsible for each crater and hence reinterpret the cometary dust size distribution [8].

References

[1] Steinbach J, Blum J, Krause M. Development of an optical trap for microparticle clouds in dilute gases. Eur. Phys. J. 2004;E 15:287-291.

[2] Blum J, Schräpler R. Structure and mechanical properties of high-porosity macroscopic agglomerates formed by random ballistic deposition. Phys. Rev. Lett. 2004;93(11):115503 (4 pp).

[3] Blum J, Schräpler R, Davidsson BJR, Trigo-Rodriguez JM. The physics of protoplanetesimal dust agglomerates. I. Mechanical properties and relations to primitive bodies in the solar system. Astrophys. J. 2006;652:1768–1781.

[4] Langkowski D, Teiser J, Blum J. The physics of protoplanetesimal dust agglomerates. II. ; Low-velocity collision properties. Astrophys. J. 2008;675:764-776.

[5] Beitz E, Güttler C, Blum J, Meisner T, Teiser J, Wurm G. Low-velocity collisions of centimeter-ust aggregates. Astrophys. J. 2011;736:34(11 pp).

[6] Heim L-O, Butt H-J, Schräpler R, Blum J. Analyzing the Compaction of High-Porosity Microscopic Agglomerates. Aust. J. Chem. 2005;58:671-673.

[7] Heim L-O, Butt H-J, Blum J, Schräpler R. A new method for the analysis of compaction processes in high-porosity agglomerates. Granular Matter 2008;10:89-91.

[8] Price MC, Kearsley AT, Burchell MJ, Hörz F, Borg J, Bridges JC et al. Comet 81P/Wild 2: the size distribution of finer (sup-10 micrometre) dust collected by the stardust spacecraft. Meteoritics and Planetary Science 2010;45(9):1409-1428.

5 sicastar® particles for preparation of colloidal droplets, monolayers and colloidal crystals

Prof. Dr. Peter Schall (University of Amsterdam, Faculty of Science, Van der Waals-Zeeman Instituut),

Dr. Cordula Grüttner (micromod Partikeltechnologie GmbH)

The drying of droplets of complex fluids such as polymer solutions or colloidal dispersions involves a large number of microscopic phenomena: solvent diffusion, transfers to the vapor/medium interface, skin formation, and skin deformation. Over the last decade, there has been a great deal of scientific and technological interests in studying the flow and deposition of materials in drying droplets. As an example, the fabrication of dried milk requires the transformation of liquid droplets into a powder form using nozzles; also liquid food concentrate is atomized into droplets using spray-drying processes. Boulogne et al. presented a study, that is focussed on the drying process of droplets of different colloidal dispersions in a confined geometry. Thus green fluorescent 50 nm sicastar® particles were used as model particles to simulate the buckling and invagination process during consolidation of colloidal droplets [1].
The preparation of colloidal monolayers or colloidal crystals requires particles with a very small size distribution. 800 nm and 1.5 µm plain sicastar® particles were used for the preparation of colloidal particle monolayers at the water/alkane interface, that were transferred onto solid substrates [2]. This technique can find application in lithography using colloidal particle arrays or in membrane fabrication of narrow pore size.

Plain sicastar® particles with a diameter of 1.5 µm served as an ideal tool for the visualization of dislocation dynamics in colloidal crystals [3,4]. Laser diffraction microscopy was used to obtain an overview of the dislocation nucleation process. Figure 1 demonstrates regions of different colours that correspond to crystal lattice distortions by indentation (left image) and under homogeneous shearing (right image) [4]. Such three-dimensional images are only possible with colloidal model materials, but not with real atomic materials.

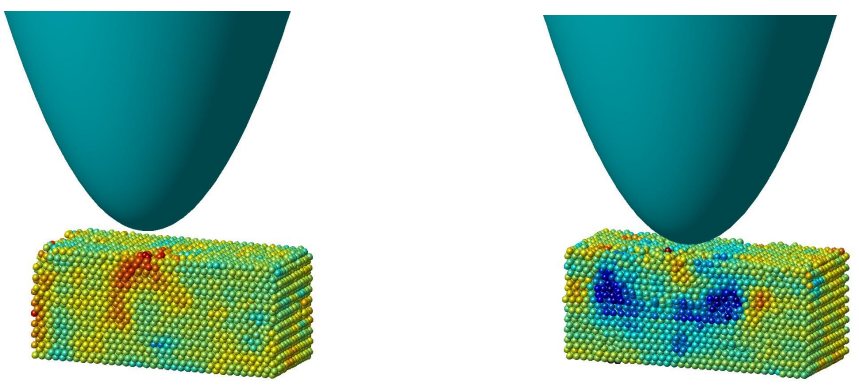

Figure 1. The colour changes demonstrate regions of different colours that correspond to crystal lattice distortions by indentation (left image) and under homogeneous shearing (right image) [4].

Einert et al. presented an experimental system, that is suitable for producing spherical crystals and for observing the distribution of lattice defects with the corresponding 1.5 µm green fluorescent sicastar® particles [5]. The introduction of fluorescent particles allowed the determination of the location and orientation of grain boundary scars.

Ramsteiner et al. presented a confocal microscopy study of the 1.5 µm plain sicastar® particles as they sediment and crystallize at the bottom wall of a container. If the particles sediment onto a feature-less flat wall, the bottom layers crystallize simultaneously and layerwise growth follows [6]. This crystallization of colloidal particles concerns the cheap and efficient large scale fabrication of photonic crystals. Subtle effects associated with the crystallization of a sediment may be exploited to induce defect structures or gradients by self- organization. Furthermore Ramsteiner et al. describe the preparation of face-centered cubic single crystals with the 1.5 µm plain sicastar® particles to study the stiffness of the crystal-liquid interface in hard-sphere colloidal systems [7]. Sicastar® suspensions quenched into the disordered state have been also used to obtain new insight into amorphous materials. Using direct tracking of the individual colloidal particles by microscopy [8,9], and x-ray scattering [10], Schall et al. obtained direct insight into basic relaxation mechanisms in the flow of glasses (Figure 2). The above studies provide excellent examples of how scientific developments can benefit from the interplay between experiments and computer simulations [6,7].

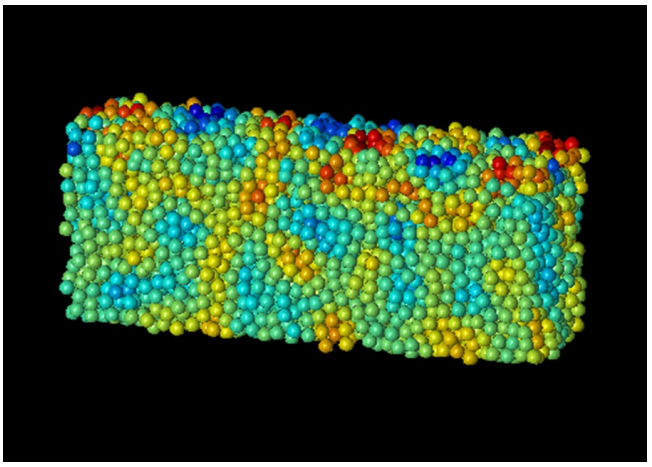

Figure 2. Structural rearrangements at the particle scale [8]

Colloidal particles dispersed in a liquid crystal (LC) host play an important role in LC nanotechnology. Oh-e et al. studied the dielectric relaxation of a pure LC in comparison to its mixtures with plain 10 µm sicastar® particles by terahertz time-domain spectroscopy [11]. They found that topological defects and structures in LC/ colloid systems are accompanied by a change of the bulk properties of the liquid crystal. The colloidal particles break the LC orientation domains, giving a very stable reproducible sample for interparticle distances < 40 µm. The measurement of the frequency dependent complex refractive index of a pure LC and of its mixtures with plain 10 µm sicastar® particles showed, that the refractive index of the pure LC was found to vary markedly due to distinct oriented domains within the sample, while the LC colloids provide very stable and reproducible spectra. These findings provide a deep insight into the fundamental changes of physical properties that occur by confining and dispersing soft condensed matter such as liquid crystals [12].

Another application of colloidal silica particles is the preparation of Gallium metallic photonic crystals. Therefore opals of 300 nm plain sicastar® particles were prepared as matrix for the infiltration of liquid gallium. Electrical and optical measurements of the gallium infiltrated opals in comparison to the bulk gallium hint at the possibility of a low frequency plasma edge [13].

References

[1] Boulogne F, Giorgiutti-Dauphine F, Pauchard L. The buckling and invagination process during consolidation of colloidal droplets. Soft Matter 2013;9:750-757.

[2] Goldenberg LM, Wagner J, Stumpe J, Paulke B-R, Görnitz E. Simple method for the preparation of colloidal particle monolayers at the water/alkane interface. Langmuir 2002;18:5627-5629.

[3] Schall P, Cohen I, Weitz DA, Spaepen F. Visualization of Dislocation Dynamics in Colloidal Crystals. Science 2004;305:1944-1948.

[4] Schall P, Cohen I, Weitz DA, Spaepen F. Visualizing dislocation nucleation by indenting colloidal crystals. Nature 2006;440:319-323.

[5] Einert T, Lipowsky P, Schilling J, Bowick MJ, Bausch AR. Grain Boundary Scars on Spherical Crystals. Langmuir 2005;21:12076-12079.

[6] Ramsteiner IB, Jensen KE, Weitz DA, Spaepen F. Experimental observation of the crystallization of hard sphere colloidal particles by sedimentation onto flat and patterned surfaces. Phys. Rev. E 2009;79:011403.

[7] Ramsteiner IB, Weitz DA, Spaepen F. Stiffness of the crystal-liquid interface in a hard-sphere colloidal system measured from capillary fluctuations. Phys. Rev. E 2010;82:41603.

[8] Schall P, Weitz DA, Spaepen F. Structural Rearrangements That Govern Flow in Colloidal Glasses. Science 2007;318:1895.

[9] Rahmani Y, Koopman R, Denisov D, Schall P. Probing incipient plasticity by indenting colloidal glasses. Scientific Reports 2013;2:1064.

[10] Denisov D, Dang MT, Struth B, Wegdam G, Schall P. Resolving structural modifications of colloidal glasses by combining x-ray scattering and rheology. Scientific Reports 2013;3:1631.

[11] Oh-e M, Yokoyama H, Koeberg M, Hendry E, Bonn M. High-frequency dielectric relaxation of liquid crystals: THz time-domain spectroscopy of liquid crystal colloids. Optics Express 2006;14(23):11433-11441.

[12] Oh-e M, Yokoyama H, Koeberg M, Hendry E, Bonn M. Liquid crystal colloids studied by THz time-domain spectroscopy. Mol. Cryst. Liq. Cryst. 2008;480:21-28.

[13] Kozhevnikov VF, Diwekar M, Kamaev VP, Shi J, Vardeny ZV. Fabrication and properties of gallium metallic photonic crystals. Physica B: Condensed Matter 2003;338(1-4):159-164.

6 sicastar® particles in optics

Dr. Frank Lüthen (University of Rostock, Department of Cell Biology),

Dr. Cordula Grüttner (micromod Partikeltechnologie GmbH)

6.1 High-resolution fluorescence microscopy based on a cyclic sequential multiphoton (CSM) process

Silica particles are interesting model particles for testing and improving microscopic techniques. Isobe et al. demonstrated the advantages of high-resolution fluorescence microscopy based on a cyclic sequential multiphoton (CSM) process in comparison to confocal microscopy. Therefore avidin-coated 3 µm sicastar® particles were labeled with biotinylated Dronpa-3. Dronpa-3 is a reversible photoswitchable fluorescent protein. The Dronpa-3-coated spheres were spin-coated on the surface of a glass slide. The fluorescence images obtained by CSM and confocal microscopy demonstrate the higher spatial resolution of the CSM image in comparison to the confocal microscopy image. Strong signals in the central region of the sphere were found in the confocal image in contrast to weak signals in the CSM image. The fluorescent Dronpa-3 was only coated on the surface of the non-fluorescent sicastar® particles. Thus fluorescence should not be generated from the central region (Figure 1) [1]. The CSM excitation technique can also be applied to various multicolor microscopies employing the sequential excitation of two processes in a single molecule. It will be an important tool in the future for investigating biological phenomena.

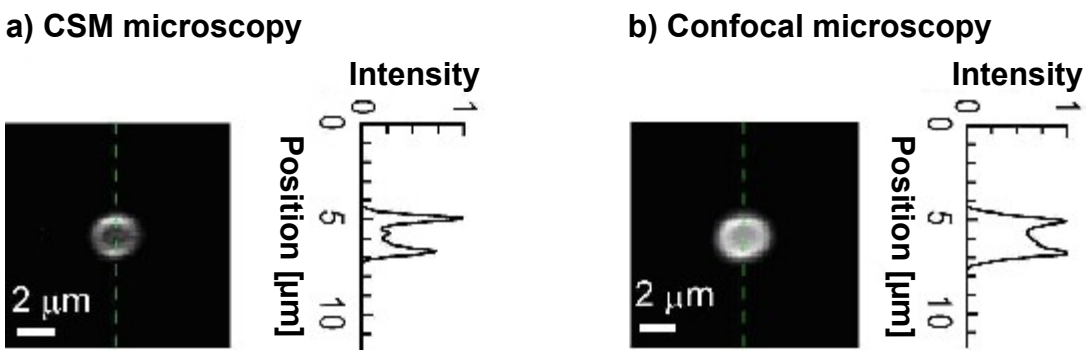

Figure 1. Fluorescence images of a Dronpa-3-coated sicastar® particles obtained by (a) CSM and (b) confocal microscopy, and intensity profiles along the green dotted lines shown in the images. Only the surface of the 3 µm diameter sphere was coated with Dronpa-3 [1].

6.2 Fixed sample preparation for 3D nanoscopy with stimulated emission depletion (STED) microscopy techniques

Tackling biological problems often involves the imaging and localization of cellular structures on the nanometer scale. Although optical super-resolution below 100 nm can be readily attained with stimulated emission depletion (STED) and photoswitching microscopy methods, attaining an axial resolution <100 nm with focused light generally required the use of two lenses in a 4Pi configuration or exceptionally bright photochromic fluorophores. Punge et al. described a simple technical solution for 3D nanoscopy of fixed samples: biological specimens are fluorescently labeled, embedded in a polymer resin, cut into thin sections, and then imaged via STED microscopy with nanoscale resolution. This approach allows a 3D image reconstruction with a resolution < 80 nm in all directions using available state-of-the art STED microscopes [2]. Silica particles were applied for the adjustment of the individual sections. Therefore green fluorescent 300 nm sicastar® particles with amino groups on the surface were additionally labelled with Atto 633 dye. Rat hippocampal neurons were immunostained and served as the biological test system. To facilitate the registration of neighboring xy-images within a z-stack, the cells were incubated with a diluted suspension of the two-color fluorescent sicastar® particles and then incubated in a polymer resin. The resulting polymer block was cut into 75-100 nm thick slices, which were transferred to the coverslip for imaging. The 300 nm sicastar® beads were also cut during sample sectioning and then identified in two to four consecutive slices, allowing the overlapping of the images taken from the different slices with high presicion. This new technique of resin embedding of biological samples, and slicing could well become a standard sample preparation in far-field fluorescence nanoscopy because of its compatibility with existing STED microscopes [2].

The same two-color 300 nm sicastar® particles were used to align the two color channels in an improved dual-color STED microscopy technique at 30 nm focal-plane resolution [3]. The imaging of two fluorophore species of different color in the same object is a major quest in far-field fluorescence nanoscopy. Meyer et al. demonstrated the ability of STED microscopy to resolve about 25-35 nm in two channels and apply this resolution to the imaging of nanometer-sized features inside cells. This increase in resolution was achieved by careful adapting the laser systems to the photochemistry of the red dye and by optimization of the optical system [3].

6.3 Manipulation of silica particles with holographic tweezers

Aberrations in biological micromanipulation images are introduced not only by the optical system, but also by the immersion liquid. Whereas optical system aberrations are constant and easily to measure, the immersion caused aberrations are variable in time and space. Reicherter et al. developed a method using 10 µm sicastar® particles as an artificial point source for aberration control. A particle is positioned by holographic optical tweezers at the location of the biological sample. The optical tweezers are based on computer generated holograms, written into spatial light modulators, which create light traps for the microparticle in the object plane. The light traps can be moved without moving any mechanically moving parts, just by changing the hologram [4]. The particle strongly focuses the light, therefore an artificial point source in the object space is created. This integration with holographic tweezers is advantageous since it offers flexibility in positioning and imaging the particles for dynamic correction of aberrations in microscopic imaging [4].

The manipulation of 10 µm sicastar® particles with holographic optical tweezers was applied to translate and rotate planar silicon membranes in solution [5]. Silicon nanomembranes are flexible, single-crystalline sheets with thicknesses ranging from less than ten up to several hundreds nanometers. These materials are extremely attractive for use in fast-flexible-electronic, optoelectronic, and nanophotonic applications. Successful integration of these nanomembranes with unique properties into next-generation devices will require new paradigms for their assembly. As nanomembranes are made thinner and thus become more difficult to handle, mechanical means of manipulation are limited in their precision with regards to controllably placing individual membranes. Oerlein et al. demonstrated the use of holographic optical tweezers for trapping and manipulating silicon nanomembranes [5]. Three-dimensional control of the nanomembranes was achieved by attaching an aminated 10 µm sicastar® particle to the silicon membrane surface. A single suspended bead was stably trapped at a power of approximately 300 mW and the nanomembrane moved towards it using a motorized microscope stage. The bead was directed to near the desired attachment point and slowly brought to the edge of the nanomembrane using the microscope stage. A strong van der Waals attraction caused immediate attachment between amino groups on the particle surface and the oxidized silicon surface of the membrane (Figure 2). Once attached, the bead functions as a nanoscale trailer hitch, facilitating manipulation of the bead together with the nanomembrane in a solution over large distances (Figure 3). This functionalized-bead handle technique could eventually enable more advanced non-contact nanofabrication using nanomembranes as building blocks for two- and three-dimensional optical and electronic devices [5].

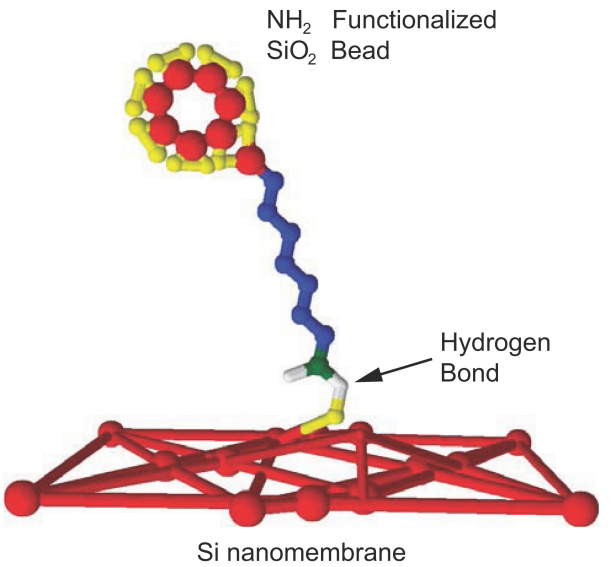

Figure 2. Depiction of the bond that forms between the bead and the silicon nanomembrane. A single bond is depicted for clarity. The bead surface is functionalized with NH2 groups and the Si surface was oxidized [5].

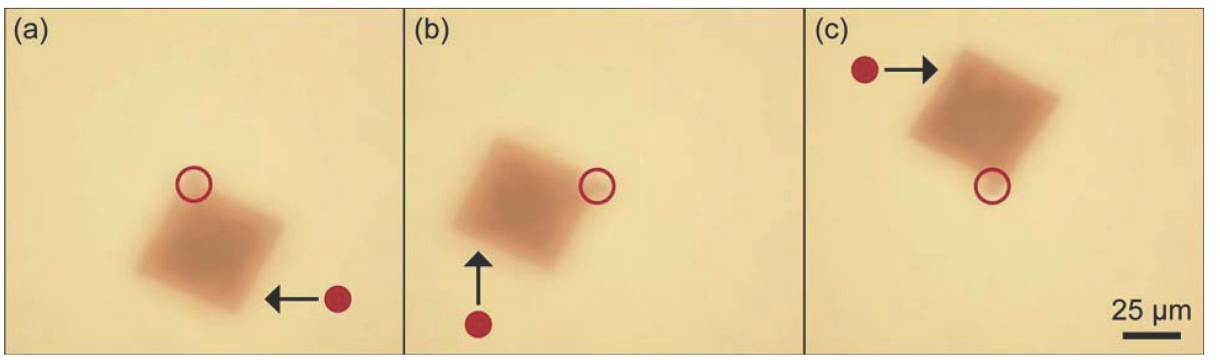

Figure 3. Extracted video frames showing laser actuated rotation of an optically trapped silicon membrane. The silicon membrane is held in place using a single static trap directed at the attached functionalized bead. Frames (a) to (c) show membrane rotation about this coordinate using a second dynamic optical trap. The second trap does not directly interact with the nanomembrane but instead uses the optical scattering force to direct its motion [5].

6.4 Mechanical characterization of free standing silica particles situated in a high resolution field emission scanning electron microscope

Understanding mechanical properties on a nanometer scale is crucial for various applications, including microelectronics, sensors, and many applications in the field of particle technology and materials science. Although mechanical properties have to be known precisely to design suitable long living products, the mechanical responses of small structures to applied loads are poorly understood. This is especially true for nano-particulate systems, caused by the experimental difficulties to test these small structures individually. Romeis et al. reported on the development of a novel *in situ* manipulator for mechanical characterization of free standing structures situated in a high resolution field emission scanning electron microscope. Plain 500 nm sicastar® particles were cast onto pieces of a standard silicon wafer by a dip-coating procedure to achieve a sufficient amount of well separated particles in the lateral scan range of the nanomanipulator on the substrate. After an appropriate positioning of the flat punch indenter over a single particle and subsequently blanking a 5 keV electron beam a load was applied by a movement of the diamond flat punch in the normal direction. To study the deformation behavior of single silica nanoparticles multiple loading experiments were conducted. Side view images recorded immediately after finishing a loading experiment give valuable feedback: measured deformation can be checked and any erroneous probe sample alignment can be excluded (Figure 4).

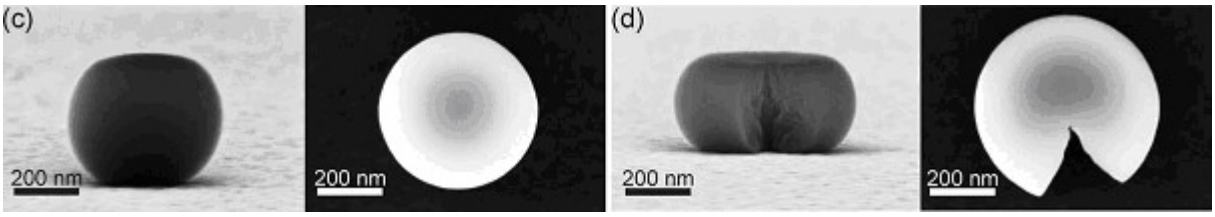

Figure 4. Force – deformation plots of silica particles. A displacement burst at a relative deformation of 0.40 ± 0.04 was observed at loads of 523 ± 46 µN. Side and top view images of the corresponding particles (c, d) reveal the connection of the burst to cracking in the meridian plane of the particles [6].

In contrast to already existing devices and well-established concepts, the novel concept for a SEM supporting stressing apparatus broadens the measuring range by a simple adjustment of the spring based force sensor. Force calibration was performed using the eigenfrequency of the force sensor inside the SEM, right before experiments are carried out. Measured deformation data are of very high accuracy, since displacements are recorded above as well as below the specimen. Based on the unique design of the apparatus an easy to validate two-springs-in-series model can be used to remove the detrimental influence of apparatus compliance on measured data. Based on the applied spring, a force resolution below 100 nN accompanied by sample deformation measurements with an accuracy of 5 nm can be achieved [6].

References

[1] Isobe K, Suda A, Hashimoto H, Kannari F, al. e. High-resolution fluorescence microscopy based on a cyclic sequential multiphoton process. Biomedical Optics Express 2010;1(3):791-797.

[2] Punge A, Rizzoli SO, Jahn R, Wildanger JD, Meyer L, Schönle A et al. 3D Reconstruction of high-resolution STED microscope images. Microsc. Res. Techniq. 2008;71:644-650.

[3] Meyer L, Wildanger D, Medda R, Punge A, Rizzoli SO, Donnert G et al. Dual-color STED microscopy at 30-nm focal-plane resolution. Small 2008;4(8):1095-1100.

[4] Reicherter M, Gorski W, Haist T, Osten W. Dynamic correction of aberrations in microscopic imaging systems using an artificial point source. SPIE USE 2004;3:5462-11.

[5] Oehrlein SM, Sanchez- Perez JR, Jacobson R, Flack FS, Kershner RJ, Lagally MG. Translation and manipulation of silicon nanomembranes using holographic optical tweezers. Nanoscale Res Lett 2011;6.

[6] Romeis S, Paul J, Peukert W. A novel apparatus for in situ compression of submicron structures and particles in a high resolution SEM. Rev. Sci. Instrum 2012;83:095105.

7 Magnetic silica particles for radionuclide extraction

Dr. Cordula Grüttner (micromod Partikeltechnologie GmbH)

The recovery of lanthanides and actinides from high level nuclear waste is an area of world-wide concern. Current approaches are based on the TRUEX process which utilizes the highly efficient, neutral, organophosphorous ligand octyl phenyl N,N-disobutyl carbamoylmethyl phosphine oxide (CMPO). Such CMPO moieties were incorporated at the wide rim of calix[4]arenes. This preorganization of the chelating CMPO ligands at the cup-shaped calixarene lead to a 100 fold increase in extraction efficiency combined with an enhanced selectivity for actinides and lighter lanthanides [1]. Solvent extraction methods using either simple or calix[4]arene-based systems, despite being highly efficient, do not lead to a marked decrease in waste volume and require large volumes of organic solvents. The application of magnetic particles has a high potential to circumvent these drawbacks. With a special surface design magnetic particles combine the selectivity of a solvent exchange ligand system with improved separation using the magnetically assisted chemical separation (MACS). After binding radionuclides the magnetic particles can be separated with a magnetic system, stripped to enable re-use, or vitrified.

Our 6 µm sicastar®-M particles were conjugated to calix[4]arenes bearing four CMPO moieties at the wide rim. The comparison of the extraction capacity for europium, americium and cerium of the CMPO-calix[4]arene bearing particles in comparison to particles with the same amount of simple CMPO ligands showed a significantly higher level of extraction of all radionuclides studied. This demonstrates the importance of pre-organization of the chelating ligands on a suitable macrocyclic scaffold, prior to their attachment at the particle surface [2].

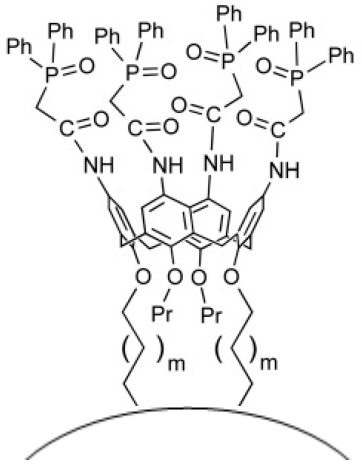

Figure 1. sicastar®-M particles with CMPO-bearing calix[4]arenes on the surface

Highly porous sicastar®-M particles with a diameter of 100 µm have a larger area for the immobilization of the chelator per g of particles than the non-porous particles. Therefore porous sicastar®-M particles were specially developed and conjugated to CMPO-containing calix[4]arenes via different spacer lengths between calixarene and particle surface (Figure 1).

In comparison to solvent extraction methods a more efficient extraction of americium and europium from simulated nuclear waste conditions has been achieved [3]. In addition surprisingly high levels of cerium could be extracted with the magnetic particles. It was also demonstrated that shorter spacer lengths of three to five carbon atoms lead to a more efficient extraction of europium and americium than the highly flexible spacer of 10 carbon atoms due to additional intermolecular interaction between CMPO units of neighboring calixarenes. But the increasing spacer length to C10 results in an increasing selectivity of the sicastar®-M particles for americium over europium due to complex formation with the CMPO units of single calixarenes. Thus the optimal spacer length for calixarene attachment on a particle surface must prevent interactions between the CMPO units of different calixarenes for a complete exploitation of the pre-organization effect of the CMPO chelators [4] The possibility of recycling the magnetic particles was demonstrated for back extraction of europium from the particle surface. The complexation capacity of the particles did not change within four complexation-back extraction cycles, that makes the magnetic particles interesting for economic industrial nuclear waste water cleaning [3,4].

Another strategy for the design of magnetic particles for an efficient binding of radionuclides is the attachment of dendrimers with a high number of terminal amino groups on the surface of our porous 100 µm sicastar®-M particles. The dendrimer-coated magnetic particles were used as a universal platform for the covalent binding of CMPO (Figure 2)[5], tripodal CMPO compounds and other selective chelators for radionuclides [6]. The introduction of the dendrimer spacers led to a 50 to 400-fold increase in europium and americium extraction in comparison with corresponding chelator-coated particles without the dendrimer spacers.

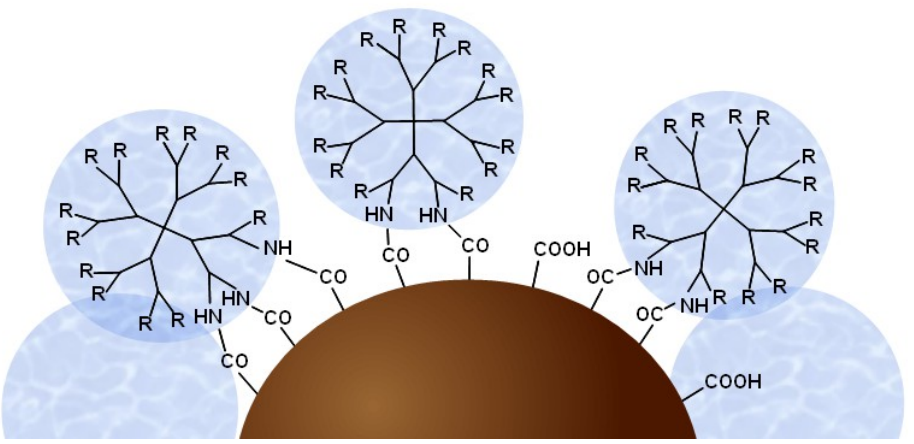

Figure 2. sicastar®-M particles with CMPO-bearing dendrimers on the surface (R=CMPO)

Back-extraction experiments with CMPO-bearing dendrimer-coated sicastar®-M particles demonstrated the possibility of multiple particle use, which also makes the application of CMPO-dendrimer coated particles an interesting alternative to conventional liquid-liquid extractions [5].

References

[1] Arnaud-Neu F, Böhmer V, Dozol J-F, Grüttner C, Jakobi RA, Kraft D et al. Calixarenes with diphenylphosphoryl acetamide functions at the upper rim. A new class of highly efficient extractants for lanthanides and actinides. J.Chem.Soc.Perkin Trans.2 1996:1175-1182.

[2] Matthews SE, Parzuchowski P, Garcia-Carrera A, Grüttner C, Dozol J-F, Böhmer V. Extraction of lanthanides and actinides by a magnetically assisted chemical separation technique based on CMPO-calix[4]arenes. Chem. Commun. 2001:417-418.

[3] Grüttner C, Rudershausen S, Matthews SE, Wang P, Böhmer V, Dozol J-F. Selective extraction of lanthanides and actinides by magnetic silica particles with CMPO-modified calix[4]arenes on the surface. Eur. Cells Materials 2002;3:48-51.

[4] Böhmer V, Dozol J-F, Grüttner C, Liger K, Matthews SE, Rudershausen S et al. Separation of lanthanides and actinides using magnetic silica particles bearing covalently attached tetra-CMPO-calix[4]arenes. Org. Biomol. Chem. 2004;2:2327-2334.

[5] Grüttner C, Böhmer V, Casnati A, Dozol J-F, Reinhoudt DN, Reinoso-Garcia MM et al. Dendrimer-coated magnetic particles for radionuclide separation. J Magn Magn Mat 2005;293:559-566.

[6] Reinoso-Garcia MM, Janczewski D, Reinhoudt DN, Verboom W, Malinowska E, Pietrzak M et al. CMP(O) tripodands: synthesis, potentiometric studies and extractions. New J. Chem. 2006;30:1480-1492.

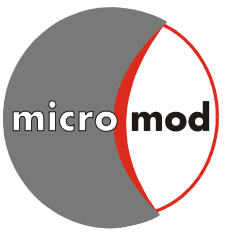

Editor:
micromod Partikeltechnologie GmbH

Registergericht: Amtsgericht Rostock HRB 5837
Steuernummer: 4079/114/03352
Ust-Id Nr. (Vat No.): DE167349493

Compilation date - September the 19th, 2013
micromod Partikeltechnologie GmbH

www.micromod.de

micromod Partikeltechnologie GmbH
Friedrich-Barnewitz-Staße 4, D-18119 Rostock
Tel.: +49 381/54 34 56 10, Fax: +49 381/54 34 56 20
E-mail: info@micromod.de, Internet: www.micromod.de